analytical chemistry

Article

pubs.acs.org/ac

Cavity-Enhanced Raman Spectroscopy of Natural Gas with Optical Feedback cw-Diode Lasers

Michael Hippler*

Department of Chemistry, University of Sheffield, Sheffield S3 7HF, United Kingdom

ABSTRACT: We report on improvements made on our previously introduced technique of cavity-enhanced Raman spectroscopy (CERS) with optical feedback cw-diode lasers in the gas phase, including a new mode-matching procedure which keeps the laser in resonance with the optical cavity without inducing long-term frequency shifts of the laser, and using a new CCD camera with improved noise performance. With 10 mW of 636.2 nm diode laser excitation and 30 s integration time, cavity enhancement achieves noise-equivalent detection limits below 1 mbar at 1 bar total pressure, depending on Raman cross sections. Detection limits can be easily improved using higher power diodes. We further demonstrate a relevant analytical application of CERS, the multicomponent analysis of natural gas samples. Several spectroscopic features have been identified and characterized. CERS with low power diode lasers is suitable for online monitoring of natural gas mixtures with sensitivity and spectroscopic selectivity, including monitoring H_2, H_2S, N_2, CO_2, and alkanes.

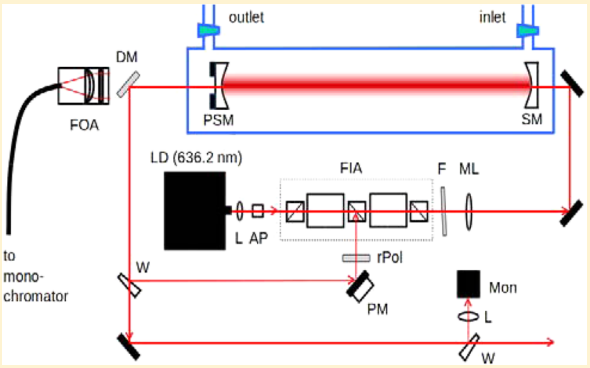

Multicomponent analysis in the gas phase is an important, but difficult, task in analytical chemistry when some components are at great excess and others are at trace levels. This is particularly relevant for monitoring natural gas which may contain different trace compounds, some of them toxic, at varying concentrations depending on the source. Common analytical techniques for multigas monitoring include gas chromatography (GC) or mass spectrometry (MS); while sensitive and selective, they require expensive equipment and have practical limitations, including difficulties detecting certain components and the need for sample preparation which prevents real-time, *in situ* monitoring. GC is a sequential technique with long analysis time, and MS has difficulties distinguishing relevant isomers.

Spectroscopic techniques are indispensable in analytical applications since they are nonintrusive, require little or no sample preparation, provide real-time data, and allow *in situ* monitoring with spectroscopic selectivity and unprecedented sensitivity.[1−12] Direct absorption techniques, like FT-IR or diode laser near-IR spectroscopy, are widely used in analytical chemistry, but some molecules are quite difficult to detect, for example, diatomic homonuclear molecules such as H_2 or N_2. This is of particular relevance for monitoring natural gas, where these gases can be minor components, or for monitoring the purity of biofuels or hydrogen gas produced by biotechnology or by alternative energies.

Due to different selection rules, Raman spectroscopy can monitor all relevant components.[12−17] The spectroscopic peaks in the Raman spectrum can be used for conclusive identification of single compounds or of individual components in mixtures. Applications of Raman spectroscopy for trace gas analysis, however, have not found widespread use so far due to the inherent weakness of Raman transitions and are thus mainly employed in condensed phases. Raman detection of natural gas has been demonstrated before, but high power lasers and high sample pressures are needed to achieve sensitivity.[13−17] Trace gas Raman spectroscopy at atmospheric pressure requires special Raman techniques which often need large laser systems and sophisticated equipment. Methods to increase sensitivity include stimulated Raman techniques such as PARS (photoacoustic stimulated Raman spectroscopy) and CARS (coherent anti-Stokes Raman spectroscopy) and fiber-enhanced or cavity-enhanced Raman spectroscopy.[12,18−26]

We have recently introduced a sensitive Raman technique where an inexpensive diode laser of low or moderate power is enhanced by several orders of magnitude in a high-finesse optical cavity.[24] Cavity-enhanced Raman spectroscopy with optical feedback diode lasers (CERS) is very selective due to high spectral resolution, and its high sensitivity allows trace gas detection in multicomponent analysis. In this contribution, we describe advancements made on this technique which improves the optical stability and improves previously reported detection limits. We further introduce a relevant analytical application of the CERS technique, the multicomponent analysis of natural gas samples, and demonstrate that CERS with low power diode lasers is suitable for online monitoring of natural gas mixtures, including monitoring H_2, H_2S, N_2, CO_2, and alkanes.

Received: April 19, 2015
Accepted: July 10, 2015
Published: July 10, 2015

DOI: 10.1021/acs.analchem.5b01462
Anal. Chem. 2015, 87, 7803−7809

EXPERIMENTAL SECTION

The experimental setup (Figure 1) is based on our previously reported CERS experiment (ref 24) but with modifications and

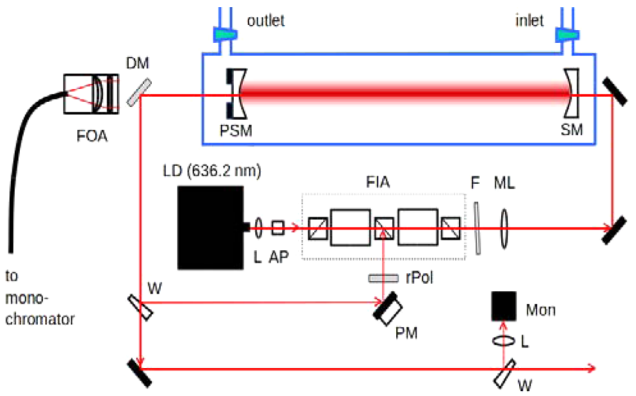

Figure 1. Scheme of the experimental setup (see main text for details).

improvements. The setup consists of a Fabry-Pérot cw-diode LD lasing single mode at 636.18 nm (Hitachi HL6322G, 80 mA, 15 °C) in a temperature stabilized mount. After collimation by an aspheric lens L, the laser beam profile is made circular by an anamorphic prism pair AP. Unwanted back reflections into the laser are prevented by an assembly of two Faraday isolators (OFR, 30-36 dB isolation each) FIA, which consists of two Faraday rotators, an entry and exit polarizer, and a polarizer between the rotators. The middle polarizer is a polarizing beam splitter which is also used for injection seeding of the diode by optical feedback. The spectrum of the diode also has a broad emission around 730 nm; to avoid this interference, a short-pass filter F (cutoff wavelength of 650 nm) removes this component. The laser radiation is coupled into a linear optical cavity by a mode matching lens ML with focus length f = 100 cm at a distance of 50 cm to the center of the cavity, effectively narrowing the beam diameter for optimal transmission. After the mode matching lens, the laser has a power of about 10 mW.

The optical cavity is composed of two concave high-reflectivity mirrors SM and PSM (Newport SuperMirrors, R > 99.99%, 1 m curvature), 35 cm apart. The mirror PSM is mounted on a piezoelectric transducer which allows fine-adjusting the cavity length to the laser wavelength (mode matching, see below). After the cavity, a dichroic mirror DM (Semrock RazorEdge) separates the excitation laser from Raman signals which are coupled into a multimode glass fiber and transferred to the monochromator. Part of the laser light is diverted back to the diode for optical feedback and locking of the diode to the cavity. This is done via a glass wedge W and a rotating polarizer rPol to adjust its intensity; one of the mirrors PM in this feedback loop is mounted on a piezoelectric transducer for phase matching (see below). A further glass wedge W diverts part of the laser light to a photodiode Mon to monitor the excitation light intensity. The optical cavity is inside a vacuum-tight glass enclosure with glass windows (BK7) and gas inlet and outlet taps which allow controlled filling of the cell with a gas mixture. Gas pressures are monitored with capacitance manometers.

The laser wavelength has to match the cavity length for efficient coupling and power buildup of light (mode matching). To achieve this, the diode injection current and laser wavelength is modulated at 2 kHz using a sawtooth waveform around one fixed cavity mode; in each cycle, the wavelength changes until it is locked to a longitudinal mode of the cavity by optical feed back. During locking, light intensity is coupled into the cavity and power builds up to a resonance; on the basis of the finesse of the cavity, we estimate a power build up by up to 3 orders of magnitude.[9,24] Within each cycle, locking continues until the resonance is lost. A suitable current offset and modulation depth is chosen so that the resonances occur in the middle of each period with a duty cycle of ca. 60%. Over time, the resonances will slowly move out of the middle position due to external perturbations; to correct for this, a lock-in amplifier of the monitored light intensity locked to the modulation derives an error signal. In our previous implementation, this error signal was added as an offset to the modulation current, readjusting the center laser wavelength to the cavity length. This can lead, however, to an accumulation of offset and long-term wavelength drift which affects the Raman calibration or may even drive the laser to a region where it is mode-hopping. In the current, improved setup, the error signal is applied after suitable amplification to the piezoelectric transducer of one of the cavity mirrors, PSM, thus leaving the laser at its center wavelength and rather adjusting the cavity length. The feedback loop itself must also be a multiple of the laser wavelength in order that constructive interference within the diode leads to efficient feedback. This phase matching is accomplished by a second, home-built electronic circuit which provides an error signal controlling the piezo-actuator of the mirror PM, based on a design described in ref 8. Both mode matching and phase matching procedures are described in more detail in our previous publications.[9,24]

Raman light scattered from within the excitation volume along the line of laser excitation is collected in a 0° forward scattering geometry, with linearly polarized excitation and unpolarized Raman detection since no analyzer was used. Raman light is imaged from the multimode glass fiber into the 100 μm entrance slit of the monochromator (Shamrock SR-750-A). An additional long pass filter (Semrock RazorEdge) further suppresses the remaining 636 nm excitation light. The spectrometer is equipped with a 1200 lines/mm high resolution grating blazed at 750 nm (specified resolution 0.04 nm) and a CCD camera (Andor iDus DU420A-OE, thermo-electrically cooled to −80 °C). Raman shifts between 400 and 5000 cm^{-1} can be measured in 500 cm^{-1} intervals with about 0.8 cm^{-1} resolution. The quantum efficiency (QE) of the grating/camera combination peaks around 750 nm with about 45%. In the Raman range of 1000−3000 cm^{-1}, QE is between 40% and 45%, tailing off to about 25% at 4200 cm^{-1}. Unless indicated otherwise, spectra and intensities are not QE corrected. Wavelength calibration is accomplished using known emission lines from a Ne/Ar lamp (ref 27) and verified by comparing methane spectra with simulations (ref 28). Raman shifts are estimated to be accurate to ±0.3 cm^{-1}. All spectra have been obtained at 30 s integration time. After subtraction of the background, intensity is converted to counts per second. Linearity of Raman signals vs concentration has been verified using ethane and H_2S Raman transitions. Further details can be found in our previous CERS publication.[24]

Natural gas was sampled on two occasions ("A" on 13/3/2015 and "B" on 16/3/2015) from different gas taps within the PC teaching laboratory of the University (gas supplied via National Grid, UK). Calibration gases include methane (CK gas, 5.0), hydrogen (CK gas, 6.0), ethane (Aldrich, 99+%),

DOI: 10.1021/acs.analchem.5b01462
Anal. Chem. 2015, 87, 7803−7809

propane (BOC industrial gases, unspecified purity), hydrogen sulfide (Sigma-Aldrich, 99.5+%), CO_2 (sublimed from dry ice), and standard laboratory air, used without further purification. All spectra were taken at room temperature, around 20 °C.

RESULTS AND DISCUSSION

CERS of Natural Gas and Its Main Constituents. Figure 2 shows an overview CERS spectrum of 1 bar of natural gas

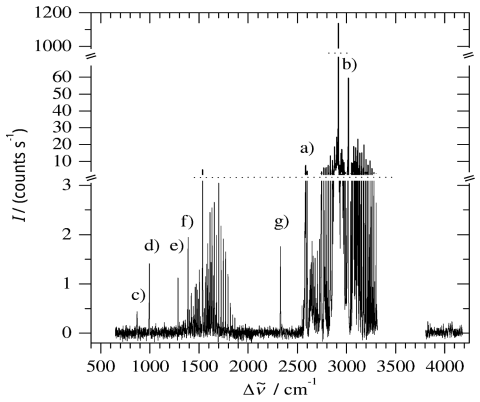

Figure 2. CERS spectrum of 1 bar natural gas sample "A". Note that the *y*-axis is split into three regions to show details more clearly. (a) and (b) are features due to methane and (c) to (g) are due to minor components; see text for more details.

sample "A". As expected, the spectrum is dominated by methane absorptions, but additional components are also apparent upon closer inspection. Since it is known that natural gas typically contains a high percentage of methane and lower admixtures of nitrogen, carbon dioxide, and higher alkanes in varying degrees depending on the source, we have measured reference spectra of pure methane, CO_2, ethane, propane, and air to obtain band positions and calibrated intensities which can be used to quantify these components in the natural gas sample analyzed.

The CERS spectrum of 1 bar methane is displayed in Figure 3. Vibrational levels of CH_4 are affected by strong rovibrational

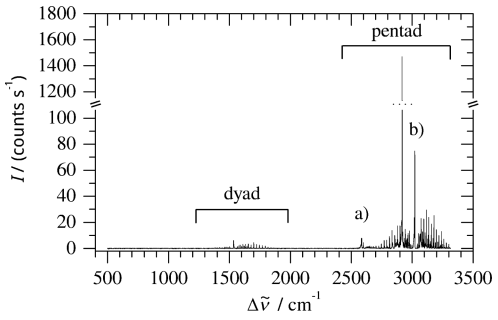

Figure 3. CERS spectrum of 1 bar of methane, for comparison with the natural gas spectrum. Features (a) and (b) are labeled as in Figure 2.

and anharmonic interactions between vibrational modes.[24,29−32] The region of the CH-bending vibrations near 1550 cm^{-1} has two interacting bands (dyad), the CH-bending fundamentals ν_2 and ν_4. This region extends from ca. 1200−2000 cm^{-1}. The region of the CH-stretching fundamentals near 3000 cm^{-1} has five interacting bands (pentad), the CH-stretching fundamentals ν_1 and ν_3, the CH-bending overtones $2\nu_2$ and $2\nu_4$, and the combination band $\nu_2 + \nu_4$. The pentad region extends from ca. 2400−3400 cm^{-1}. Its Raman spectrum is dominated by the *Q*-branch of the totally symmetric ν_1 band at 2916.7 cm^{-1}. The pentad has also some weaker transitions, e.g., transitions to the A_1 component of $2\nu_4$ near 2585 cm^{-1} (labeled a) in Figures 2 and 3) or transitions to the F_2 component of ν_3 near 3020 cm^{-1} (labeled b) in Figures 2 and 3). These transitions also appear in a simulation of the CH_4 Raman spectrum by the STDS program and molecular parameters from the Dijon group.[28] In a previous discussion of Raman spectra of natural gas by Hansen et al.,[13] features observed at 3020 cm^{-1} have been assigned to methane, in agreement with our work, but a feature near 2585 cm^{-1} has been assigned to H_2S, with a rather high, unexpected abundance. On the basis of our observation here, it appears likely that this feature is rather due to methane, too (see also discussion below on H_2S). The isotopomer $^{13}CH_4$ has a natural abundance of 1.1%. A simulation of its theoretical spectrum shows that, at natural abundance, its features will be hidden under much stronger $^{12}CH_4$ features. Higher spectral resolution will be beneficial for methane isotope studies to resolve features better.

Figure 4 shows the CERS spectrum of 1 bar of lab air (assuming standard 78% N_2 and 21% O_2 by volume). The *Q*-

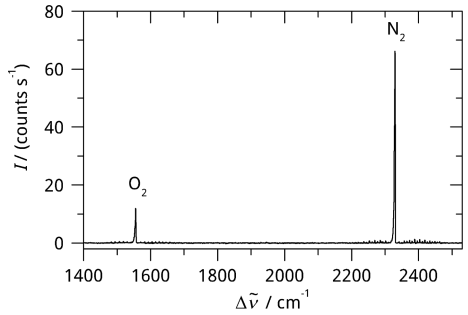

Figure 4. CERS spectrum of 1 bar of lab air, showing the prominent *Q*-branch contours of the O_2 and N_2 fundamentals.

branch of the $^{16}O_2$ fundamental is observed at 1555.5 cm^{-1} and the *Q*-branch of $^{14}N_2$ at 2329.0 cm^{-1}. In addition, rotationally resolved *O*- and *S*-branch transitions can be seen at much lower intensities and also the $^{14}N^{15}N$ isotopomer at natural abundance.[24] The CERS baseline has a noise level (standard deviation) of about 0.08 counts s^{-1} at the 30 s integration time, corresponding to a noise equivalent detection limit of 1.0 mbar N_2 and 1.4 mbar O_2 based on peak intensities. Detection limits based on integrated areas are expected to be lower. Detection limits reported here improve on our previously reported limits,[24] because the camera used in this study has reduced noise. Compared with the natural gas spectrum (Figure 2), it is clear that feature (g) is the *Q*-branch of nitrogen, with a partial pressure of 21 mbar or 2.1% by volume abundance in the 1 bar natural gas sample, obtained by comparing integrated areas. No evidence of oxygen is apparent in the natural gas sample within our detection limits.

The Raman spectrum of carbon dioxide is dominated by the *Q*-branches of the $\nu_1/2\nu_2^0$ Fermi resonance pair (see Figure 5),[1,33] (e) observed at 1285.1 cm^{-1} and (f) observed at 1387.7 cm^{-1}; both features have a fwhm of 1.7 cm^{-1}. Compared with the natural gas spectrum where the same features (e) and (f) have been observed (Figure 2), a partial pressure of 15 mbar CO_2 or 1.5% by volume abundance in 1 bar of gas is obtained.

DOI: 10.1021/acs.analchem.5b01462
Anal. Chem. 2015, 87, 7803−7809

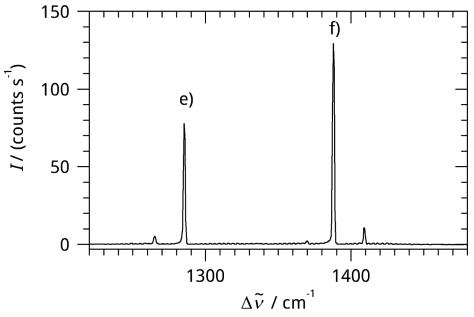

Figure 5. CERS spectrum of 1 bar CO_2. Features (e) and (f) are labeled as in Figure 2; they represent the Q-branches of the $\nu_1/2\nu_2^0$ Fermi resonance pair.

Measured CERS spectra of ethane and propane are displayed in Figure 6. The Raman spectra are dominated by CH-stretching vibrations in the 2600−3000 cm^{-1} region. They also have characteristic symmetric C−C stretching vibrations: ethane, the ν_3 (a_{1g}) with the Q-branch observed at 994.4 cm^{-1} with fwhm of 3.6 cm^{-1}, and propane, the ν_8 (a_1) with the Q-branch observed at 869.0 cm^{-1} with fwhm 4.3 cm^{-1}. The C−C stretching features have been labeled (c) (propane) and (d) (ethane) and have also been observed in the natural gas sample (Figure 2). Comparing integrated areas, partial pressures of 42 mbar (4.2%) ethane and 23 mbar (2.3%) propane in 1 bar of the natural gas sample are deduced (in parentheses abundance by volume). Higher alkanes like butane, pentane, or hexane have C−C stretching vibrations shifted to lower wavenumbers; within our detection limits (estimated 5 mbar or 0.5% for C−C stretching vibrations), they are not apparent in the natural gas spectrum.

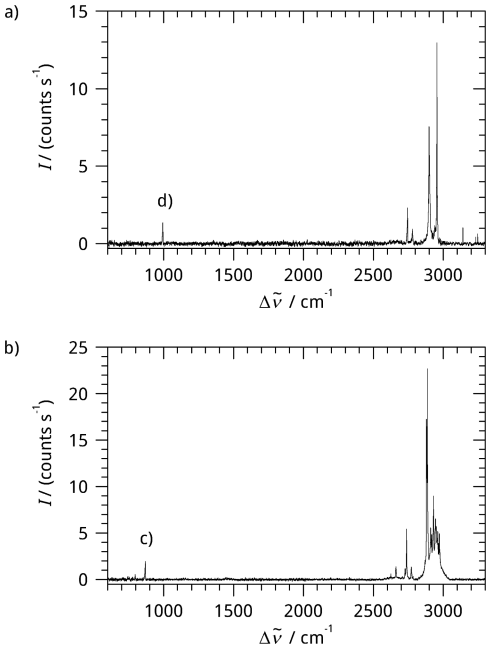

Figure 6. (a) CERS spectrum of 43 mbar of ethane; (b) CERS spectrum of 100 mbar of propane. Features (c) and (d) (labeled as in Figure 2) are the Q-branches of the C−C stretching vibrations.

In principle, better detection for alkanes can be expected in the CH-stretching vibration region, since these transitions are much stronger than the symmetric C−C stretching vibration. However, in natural gas, this region is heavily congested by methane. To demonstrate the principle of detection in the CH-stretching region, but also demonstrate the difficulties, we have subtracted methane (scaled to correspond to 0.88 bar or 88% abundance) from the 1 bar natural gas spectrum (see Figure 7).

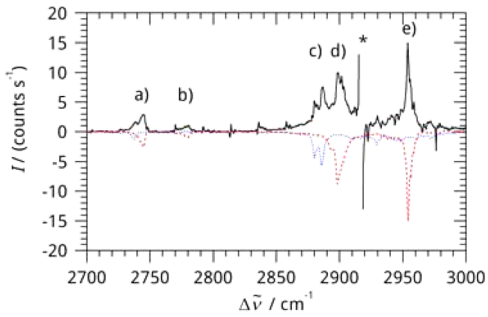

Figure 7. Difference CERS spectrum in the CH-stretching region, where 0.88 bar methane (as in Figure 2) has been subtracted from 1 bar natural gas (as in Figure 1). The red dashed line shows 50 mbar of ethane and the blue dotted line shows 25 mbar of propane (intensities mirrored). Features (a) to (e) are discussed in the main text. The asterisk denotes the region of the 2917 cm^{-1} Q-branch peak of methane, where the subtraction procedure shows artifacts.

Remaining transitions are then expected to be due to species other than methane. The 88% level of methane has been chosen because it subtracts methane peaks effectively without causing negative transitions; it is also consistent with the amount of minor other components as determined before. The subtraction procedure produces some artifacts at the position of strong methane transitions in the form of features which are oscillating around the baseline (see, eg., the region denoted by an asterisk in Figure 7), but in general, the procedure works well. As can be seen from Figure 7, the remaining transitions can be accounted for by 50 mbar ethane and 25 mbar propane, in reasonable agreement with the values determined from the C−C stretching region. Features (d) and (e) are the dominant transitions of ethane and (b) is a minor transition of ethane. Feature (c) is the dominant transition of propane, and feature (a) is a mixture of ethane and propane. Detection in the CH-stretching vibration region is qualitatively more sensitive to alkanes, but due to the artifacts introduced by the methane subtraction, it is considered to be less accurate than using the more characteristic C−C stretching region below 1000 cm^{-1}.

For convenience, spectroscopic features used for all compounds are summarized in Table 1. Note that peak heights, and to a degree also peak positions, depend on the experimental spectral resolution. Intensities cannot be directly compared to literature values (eg., refs 34 and 35), since the literature usually refers to the integrated area of an entire vibrational band, whereas in Table 1, we give peak values and integrated areas of defined features, most often the Q-branch of a vibration. The results of our analysis of sample "A" are summarized in Table 2. We have also sampled natural gas on a different day ("B", 17/3/2015) and in a different location within the department. The results are also summarized in Table 2. This sample has less N_2, CO_2, and propane but slightly more ethane. Note that the samples are not "fresh" samples, since the gas was probably standing for an unknown amount of time within the lines of the department. Note that no other components are obvious, in particular no H_2 (4100−4200 cm^{-1}) or H_2S (2610 cm^{-1}); see also the discussions in the

DOI: 10.1021/acs.analchem.5b01462
Anal. Chem. 2015, 87, 7803−7809

Table 1. CERS Raman Characteristics of Compounds Measured

compound	spectral feature	peak position (cm^{-1})	peak height (counts s^{-1})[a]	integrated area (counts s^{-1} cm^{-1})[b]	QE (%)[c]
CH_4	ν_1 Q-branch	2916.7	1470	2310	40
$^{14}N_2$	Q-branch	2329.0	85	263	45
$^{16}O_2$	Q-branch	1555.5	57	210	44
CO_2	$\nu_1/2\nu_2^0$ Q-branch component (e)	1285.1	78	134	43
	component (f)	1387.7	129	212	44
ethane C_2H_6	ν_3 (a_{1g}) (C−C stretching) Q-branch	994.4	32	130	40
propane C_3H_8	ν_8 (a_1) (C−C stretching) Q-branch	869.0	19	98	38
H_2S	ν_1 (a_1) (S−H stretching) Q-branch	2610.0	820	5500	43
H_2	Q (1)	4155.3	585	599	26

[a]Peak height and area converted to correspond to 1 bar partial pressure, assuming linear response. Raman intensities refer to 0° forward scattering geometry with 636.2 nm linear excitation and unpolarized detection (see refs 24 and 36 for relation with scattering activities and cross sections). [b]Integration over Q-branch, except for H_2, where integration over Q(1) line. [c]Estimated quantum efficiency of grating/camera combination at the Raman shifted wavelength.

Table 2. Composition of Two Different Natural Gas Samples, Determined by CERS

component (% by volume)[a]	sample "A" (13/3/2015)	sample "B" (16/3/2015)
CH_4	88	92
N_2	2.1	1.3
CO_2	1.5	0.4
ethane	4.2	4.6
propane	2.3	0.5
higher alkanes	<0.5[b]	<0.5[b]
H_2S	<0.01[b]	<0.01[b]
H_2	<0.014[b]	<0.014[b]

[a]Estimated accuracy about 5% of value, limited by day-to-day laser/alignment fluctuations. [b]Below the estimated detection limits.

following paragraphs. The present results show that CERS is very useful for online monitoring of gas composition at 1 bar total pressure, with good sensitivity and accuracy. Relative sensitivity will obviously improve with higher gas pressures; the noise equivalent detection limit of 1 mbar N_2 corresponds to 0.1% in 1 bar, for example; but it would improve to 10 ppm at 100 bar total pressure, a pressure more typical for gas storage facilities and processing plants.

Hydrogen Sulfide. Hydrogen sulfide is a common minor component in natural gas, but due to its high toxicity, it is usually removed at the source and only very low trace levels are expected to be present in gas supply lines, if any. Since a previous study claims to have detected unexpected, significant levels of H_2S in Danish natural gas,[13] we decided to reinvestigate the Raman spectroscopy of H_2S. Figure 8 shows

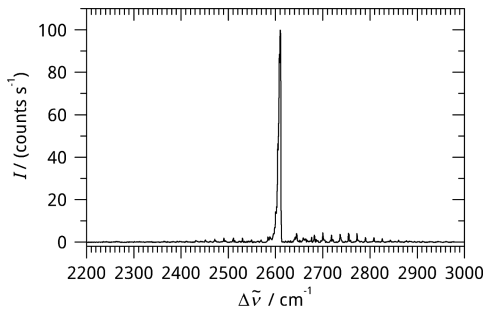

Figure 8. CERS spectrum of 122 mbar hydrogen sulfide, H_2S, with the dominant Q-branch of the symmetric S−H stretching vibration ν_1 (a_1).

part of the CERS spectrum of H_2S with the strongest transitions. The Raman spectrum is dominated by the totally symmetric ν_1 (a_1) S−H stretching vibration with a sharp and characteristic Q-branch observed at 2610.0 cm^{-1}. The peak is partially rotationally resolved, shaded toward lower wavenumbers, and has 5.6 cm^{-1} fwhm. With a baseline noise of 0.08 counts s^{-1}, a noise equivalent detection limit of 0.1 mbar is deduced on the basis of peak heights. This Q-branch has been observed before near 2610.8 cm^{-1} in the gas phase, 2573.6 cm^{-1} in the liquid phase, and 2553.7 cm^{-1} in the solid phase.[1] In the natural gas samples analyzed in the present work, no features are apparent at 2610 cm^{-1}, indicating that in our samples H_2S, if present at all, is below the detection limit. The previous study has observed features near 2585 cm^{-1} and assigned it to the S−H stretching vibration of H_2S, red-shifted from its 2610 cm^{-1} position due to the high pressures of the natural gas sampled (up to 100 bar).[13] Although red shifting is common at high densities due to molecular association (in the case of H_2S, presumably hydrogen bonding), a shift toward and even below the liquid phase value seems rather unusual in a gas sample; the authors in the previous study have therefore suggested that, at high gas pressures, H_2S may be present in the form of droplets.[13] Since we have observed CH_4 transitions near 2585 cm^{-1} (feature a) in Figures 2 and 3), it appears likely to us that rather methane has been observed in the previous study.

Simultaneous Detection of Natural Gas and Hydrogen Gas, H_2. Some natural gas sources may contain low levels of hydrogen gas, but we could not detect H_2 in our samples. With the advent of a possible hydrogen economy,[37] there have been suggestions to produce hydrogen gas by alternative, renewable energies or as biofuel produced by bacteria or algae and feed this gas into the natural gas grid or into separate gas storing facilities. In any case, there is clearly a need to detect hydrogen gas either in the pure state or as a component in a gas mixture with sensitivity and selectivity. H_2 is difficult to detect by direct absorption, but also by other techniques. Raman detection, however, seems to be an attractive alternative option.[18,19,21,24] To demonstrate the capability of CERS for the simultaneous detection of natural gas and hydrogen gas, we have prepared mixtures of these gases at 1 bar and measured them by the CERS technique. Figure 9 shows the CERS spectrum of 1 bar of pure H_2. The region near 4155 cm^{-1} has strong Raman transitions due to rotationally resolved Q-branch transitions to its fundamental vibration, with a characteristic 1:3 intensity variation between even and odd J-values due to

DOI: 10.1021/acs.analchem.5b01462
Anal. Chem. 2015, 87, 7803−7809

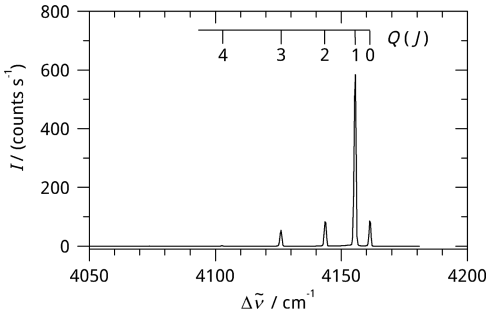

Figure 9. CERS spectrum of 1 bar H_2, with rotationally resolved *Q*-branch transitions.

nuclear spin statistics. At room temperature, the strongest transition is the $Q(1)$ line, observed at 4155.3 cm^{-1} with 1.1 cm^{-1} fwhm; with a baseline noise of 0.08 counts s^{-1}, the observed peak height corresponds to a noise equivalent detection limit of 0.14 mbar at 30 s integration time. With a Gaussian fit procedure comparing the integrated area of $Q(1)$, detection limits are expected to improve further.[24]

The CERS spectrum of a mixture of 900 mbar natural gas and 100 mbar H_2 is displayed in Figure 10; the partial pressures

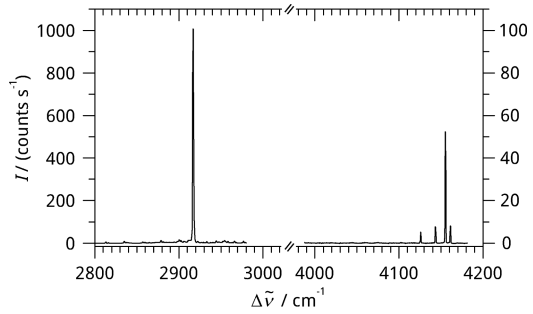

Figure 10. CERS spectrum of a mixture of 900 mbar natural gas and 100 mbar hydrogen gas. Note the different intensity scales of the left- and right-hand side of the figure.

are taken from the capacitance pressure gauge readings of the gas mixing line. Using the Raman intensity values from the H_2 measurement (Figure 9) as a calibration, the H_2 Raman intensity in the mixture indicates a partial pressure of 94 mbar, in reasonable agreement with the pressure gauge reading. This shows that CERS is suitable for multicomponent analysis of gas mixtures, including natural gas and hydrogen gas.

CONCLUSIONS

CERS has great potential as an analytical technique for the gas phase with high sensitivity. In this study, we report on improvements made on our previously introduced CERS technique for Raman spectroscopy in the gas phase, including a new mode-matching procedure which keeps the laser in resonance with the optical cavity without inducing long-term frequency shifts of the laser, and using a new camera with improved noise performance. With 10 mW of 636.2 nm diode laser excitation and 30 s integration time, cavity enhancement achieves noise-equivalent detection limits of 0.05 mbar (CH_4), 0.1 mbar (H_2S), 0.14 mbar (H_2), and 1 mbar (N_2), depending on Raman cross sections. At 1 bar total pressure, this corresponds to relative abundance by volume between 0.005% and 0.1% or 50 and 1000 ppm. Higher total pressures are more typical for gas storage facilities and gas processing plants. At 100 bar, the partial pressure detection limits would correspond to abundancies between 0.5 and 10 ppm. Detection limits can be further improved using higher power lasers.

We further demonstrated a relevant analytical application of our CERS technique, the multicomponent analysis of natural gas samples. We could successfully show that CERS with low power diode lasers is suitable for online monitoring of natural gas mixtures with sensitivity and spectroscopic selectivity, including monitoring H_2, H_2S, N_2, CO_2, and alkanes. Several spectroscopic features have been identified and characterized, including a reassignment of Raman transitions near 2585 cm^{-1} to methane.

This proof-of-concept was on mixtures at atmospheric total pressure, suitable to measure compositions at domestic gas supply lines, for example; in the future, the technique can also be extended to measure high-pressure gas by enclosing the optical cavity into a high-pressure cell. CERS signals and thus detection limits scale linearly with excitation laser power and with the Raman Stokes frequency raised to the power of four, $(\nu_{Raman})^4$. In order to increase sensitivity further, we therefore plan to use diode lasers with higher power and diodes lasing in the violet region in future work with CERS.

AUTHOR INFORMATION

Corresponding Author

*E-mail: M.Hippler@sheffield.ac.uk.

Notes

The author declares no competing financial interest.

ACKNOWLEDGMENTS

This research is sponsored by a proof-of-concept grant of the NERC (Natural Environment Research Council, UK, grant NE/I000844/1) and by the University of Sheffield.

REFERENCES

(1) Herzberg, G. *Molecular Spectra and Molecular Structure, Vol. II, Infrared and Raman Spectra of Polyatomic Molecules*, 7th ed.; Van Nostrand: Toronto, 1956.
(2) Quack, M. *Annu. Rev. Phys. Chem.* **1990**, *41*, 839−874.
(3) Sigrist, M. W. Ed. *Air Monitoring by Spectroscopic Techniques*; Chemical Analysis Series 127; Wiley: New York, 1994.
(4) Duxbury, G. *Infrared Vibration-Rotation Spectroscopy: From Free Radicals to the Infrared Sky*; John Wiley & Sons: Chichester, 2000.
(5) Brown, S. S. *Chem. Rev.* **2003**, *103*, 5219−5238.
(6) Ball, S. M.; Jones, R. L. *Chem. Rev.* **2003**, *103*, 5239−5262.
(7) Kassi, S.; Chenevier, M.; Gianfrani, L.; Salhi, A.; Rouillard, Y.; Ouvrard, A.; Romanini, D. *Opt. Express* **2006**, *14*, 11442−11452.
(8) Baran, S. G.; Hancock, G.; Peverall, R.; Ritchie, G. A. D.; van Leeuwen, N. J. *Analyst* **2009**, *134*, 243−249.
(9) Hippler, M.; Mohr, C.; Keen, K.; McNaghten, E. *J. Chem. Phys.* **2010**, *133*, 044308 (1−8).
(10) Hamilton, D. J.; Orr-Ewing, A. J. *Appl. Phys. B: Lasers Opt.* **2011**, *102*, 879−890.
(11) Hippler, M.; Miloglyadov, E.; Quack, M.; Seyfang, G. Mass and Isotope-Selective Infrared Spectroscopy. In *Handbook of High-Resolution Spectroscopy*; Quack, M.; Merkt, F., Eds.; John Wiley: Chichester, 2011; pp 1069−1118.
(12) Weber, A. High-Resolution Raman Spectroscopy of Gases. In *Handbook of High-Resolution Spectroscopy*; Quack, M.; Merkt, F., Eds.; John Wiley: Chichester, 2011; pp 1153−1236.
(13) Hansen, S. B.; Berg, R. W.; Stenby, E. H. *Appl. Spectrosc.* **2001**, *55*, 55−60.
(14) Kiefer, J.; Seeger, T.; Steuer, S.; Schorsch, S.; Weikl, M. C.; Leipertz, A. *Meas. Sci. Technol.* **2008**, *19*, 085408 (9pp).

DOI: 10.1021/acs.analchem.5b01462
Anal. Chem. 2015, 87, 7803−7809

(15) Buldakov, M. A.; Korolev, B. V.; Matrosov, I. I.; Petrov, D. V.; Tikhomirov, A. A. *J. Appl. Spectrosc.* **2013**, *80*, 124−128.
(16) Buldakov, M. A.; Korolkov, V. A.; Matrosov, I. I.; Petrov, D. V.; Tikhomirov, A. A.; Korolev, B. V. *J. Opt. Technol.* **2013**, *80*, 426−430.
(17) Eichmann, S. C.; Kiefer, J.; Benz, J.; Kempf, T.; Leipertz, A.; Seeger, T. *Meas. Sci. Technol.* **2014**, *25*, 075503.
(18) Lavorel, B.; Millot, G.; Rotger, M.; Rouillé, G.; Berger, H.; Schrötter, H. W. *J. Mol. Struct.* **1992**, *273*, 49−59.
(19) Spencer, C. L.; Watson, V.; Hippler, M. *Analyst* **2012**, *137*, 1384−1388.
(20) Hanf, S.; Keiner, R.; Yan, D.; Popp, J.; Frosch, T. *Anal. Chem.* **2014**, *86*, 5278−5285.
(21) James, T. M.; Rupp, S.; Telle, H. H. *Anal. Methods* **2015**, *7*, 2568−2576.
(22) King, D. A.; Pittaro, R. J. *Opt. Lett.* **1998**, *23*, 774−776.
(23) Taylor, D. J.; Glugla, M.; Penzhorn, R.-D. *Rev. Sci. Instrum.* **2001**, *72*, 1970−1976.
(24) Salter, R.; Chu, J.; Hippler, M. *Analyst* **2012**, *137*, 4669−4676.
(25) Keiner, R.; Frosch, T.; Massad, T.; Trumbore, S.; Popp, J. *Analyst* **2014**, *139*, 3879−3884.
(26) Thorstensen, J.; Haugholt, K. H.; Ferber, A.; Bakke, A. H.; Tschudi, J. *J. European Opt. Soc. Rapid Publ.* **2014**, *9*, 14054 (6pp).
(27) Sansonetti, J. E.; Martin, W. C.; Young, S. L. *Handbook of Basic Atomic Spectroscopic Data*; National Institute of Standards and Technology (NIST): Gaithersburg; http://www.nist.gov/pml/data/handbook/ (accessed March 2015).
(28) Wenger, Ch.; Champion, J.-P. *J. Quant. Spectrosc. Radiat. Transfer* **1998**, *59*, 471−480. ftp://jupiter.u-bourgogne.fr/dist/STDS_UNIX/ (accessed March 2015).
(29) Champion, J.-P.; Loëte, M.; Pierre, G. Spherical Top Spectra. In *Spectroscopy of the Earth's Atmosphere and Interstellar Medium*; Rao, K. N., Weber, A., Eds.; Academic Press: Boston, 1992; pp 339−422.
(30) Hippler, M.; Quack, M. *J. Chem. Phys.* **2002**, *116*, 6045−6055.
(31) Jourdanneau, E.; Chaussard, F.; Saint-Loup, R.; Gabard, T.; Berger, H. *J. Mol. Spectrosc.* **2005**, *233*, 219−230.
(32) Nikitin, A. V.; Boudon, V.; Wenger, Ch.; Albert, S.; Brown, L. R.; Bauerecker, S.; Quack, M. *Phys. Chem. Chem. Phys.* **2013**, *15*, 10071−10093.
(33) Fermi, E. *Eur. Phys. J. A* **1931**, *71*, 250−259.
(34) Fenner, W. R.; Hyatt, H. A.; Kellam, J. M.; Porto, S. P. S. *J. Opt. Soc. Am.* **1973**, *63*, 73−77.
(35) Schrötter, H. W.; Klöckner, H. W. Raman Scattering Cross Sections in Gases and Liquids. In *Topics in Current Physics, Raman Spectroscopy of Gases and Liquids*; Weber, A., Ed.; Springer Verlag: New York, 1979; Chapter 4, p 123.
(36) Long, D. A. *The Raman Effect: A Unified Treatment of the Theory of Raman Scattering by Molecules*; John Wiley & Sons: Chichester, 2002.
(37) Conte, M.; Iacobazzi, A.; Ronchetti, M.; Vellone, R. *J. Power Sources* **2001**, *100*, 171−187.

DOI: 10.1021/acs.analchem.5b01462
Anal. Chem. 2015, 87, 7803−7809